Neuron 52, 511–524, November 9, 2006 ©2006 Elsevier Inc. DOI 10.1016/j.neuron.2006.09.014

Network Variability Limits Stimulus-Evoked Spike Timing Precision in Retinal Ganglion Cells

Gabe J. Murphy[1,2,*] and Fred Rieke[1,2]
[1] Howard Hughes Medical Institute
[2] Department of Physiology and Biophysics
University of Washington
Seattle, Washington 98195

Summary

Visual, auditory, somatosensory, and olfactory stimuli generate temporally precise patterns of action potentials (spikes). It is unclear, however, how the precision of spike generation relates to the pattern and variability of synaptic input elicited by physiological stimuli. We determined how synaptic conductances evoked by light stimuli that activate the rod bipolar pathway control spike generation in three identified types of mouse retinal ganglion cells (RGCs). The relative amplitude, timing, and impact of excitatory and inhibitory input differed dramatically between On and Off RGCs. Spikes evoked by repeated somatic injection of identical light-evoked synaptic conductances were more temporally precise than those evoked by light. However, the precision of spikes evoked by conductances that varied from trial to trial was similar to that of light-evoked spikes. Thus, the rod bipolar pathway modulates different RGCs via unique combinations of synaptic input, and RGC temporal variability reflects variability in the input this circuit provides.

Introduction

Sensory stimuli evoke reproducible and temporally precise patterns of action potentials (APs) in neurons responsible for early sensory processing (reviewed in Buracas and Albright, 1999; Carr, 1993; Oertel, 1999; Petersen et al., 2002; Laurent, 1999). Rapidly changing features of time-varying tactile, auditory, and visual stimuli, for example, evoke APs that exhibit low (1–5 ms) trial-to-trial temporal variability in primary somatosensory, primary auditory, lateral geniculate, and middle temporal (MT) area neurons (Arabzadeh et al., 2005; Gabernet et al., 2005; DeWeese et al., 2003; Reinagel and Reid, 2000; Buracas et al., 1998). Variability in AP timing is generally assumed to reflect noise in the pattern and integration of synaptic input, as somatic injection of fluctuating current evokes highly reproducible and temporally precise patterns of APs in the absence of synaptic input (Mainen and Sejnowski, 1995; but see White et al., 2000).

Experiments performed in brain slices have identified multiple network and synaptic properties that facilitate the precision of APs evoked by electrical stimulation. Feedforward synaptic inhibition can truncate the temporal window during which excitatory inputs are integrated (Pouille and Scanziani, 2001), and synchronous input from GABAergic interneurons coupled by gap junctions can permit neurons to discriminate closely-timed excitatory inputs (Beierlein et al., 2000; Galarreta and Hestrin, 2001). Intrinsic mechanisms (Oertel, 1991; Trussell, 1997) and dendritic properties (Stuart et al., 2000; Magee, 2000; Reyes, 2001) can also facilitate precise spike timing and/or coincidence detection. It has proven difficult, however, to determine the mechanisms governing the precision of APs evoked by physiological stimuli in intact, active, tractable neural circuits.

The mammalian retina provides an opportunity to study in parallel the precision of light-evoked AP generation and the network and intrinsic mechanisms governing that precision. Bright fluctuating light stimuli evoke spikes with high (1–5 ms) temporal precision in retinal ganglion cells (RGCs) (Berry et al., 1997; Reich et al., 1997; Keat et al., 2001; Uzzell and Chichilnisky, 2004) but activate an incompletely understood constellation of retinal cells and circuits. Signals evoked by dim light stimuli, however, are conveyed and processed by a specific and identifiable circuit in mammalian retina—the rod bipolar pathway (reviewed by Bloomfield and Dacheux, 2001; Field et al., 2005).

Can signals carried by the rod bipolar pathway generate reproducible and precisely-timed APs in mammalian RGCs? If so, what properties of the cells and synapses that comprise the rod bipolar circuit enable and limit the precision of light-evoked AP generation? To answer these questions we (1) identified conditions under which light-evoked signals in three functionally identified RGC types are dominated by input from the rod bipolar pathway; (2) characterized the precision of APs evoked by these stimuli; and (3) measured and manipulated the light-evoked synaptic inputs to understand how they govern AP generation. These experiments revealed that the amplitude, timing, and integration of excitatory and inhibitory synaptic input differed dramatically between On and Off RGCs. In all RGCs examined, however, replacing synaptic input with repeated somatic injection of identical light-evoked synaptic conductances produced APs with substantially greater precision than APs evoked directly by light stimuli. Moreover, the temporal precision of APs evoked by somatic injection of measured synaptic conductances that varied from trial to trial closely resembled that of spikes evoked by light stimuli. These data provide direct evidence that variability in synaptic input provided by the rod bipolar pathway limits the temporal precision of light-evoked AP generation.

Results

Functional Identification of Ganglion Cells

We used infrared differential interference contrast microscopy to target ganglion cells with the largest somata (>20 μm diameter) in a flat mount preparation of the mouse retina. Consistent with previous reports (Pang et al., 2003), we encountered three functional types of ganglion cell. On cells exhibited a sustained increase in firing rate during a step increase in light intensity from darkness to 10 Rh*/Rod/s (Figure 1A). Off

*Correspondence: gjmurphy@u.washington.edu

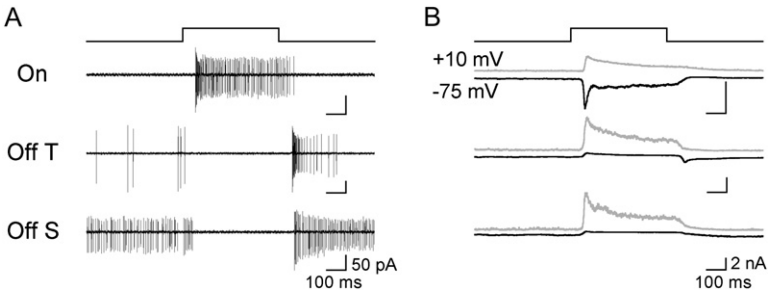

Figure 1. Functional Identification of Ganglion Cell Types

(A) Cell-attached recording of APs evoked in On, Off T, and Off S cells by a 500 ms step that generated ~10 Rh*/Rod/s.

(B) Excitatory (black, Vm = −75 mV) and inhibitory (gray, Vm = +10 mV) postsynaptic currents evoked by the same stimulus.

transient (Off T) cells generated a burst of spikes at light offset, whereas Off sustained (Off S) cells exhibited tonic firing before and after a light step (Figure 1A).

To characterize light-evoked excitatory and inhibitory synaptic input to each cell type, we performed whole-cell voltage-clamp recordings (Figure 1B). We isolated inhibitory postsynaptic currents (IPSCs) by recording at the reversal potential for excitatory postsynaptic currents (EPSCs; +10 mV), and isolated EPSCs by recording near the reversal potential for IPSCs (−75 mV). Light steps produced distinctive patterns of excitatory and inhibitory synaptic input in On, Off transient, and Off sustained cells. The large somata and characteristic light responses enabled us to distinguish these three cell types from each other and from other RGC types.

Isolation of Signals Traversing the Rod Bipolar Pathway

Signals generated in mammalian rods by dim light stimuli are conveyed to ganglion cells via at least three pathways (Figure 2A; reviewed by Bloomfield and Dacheux, 2001): (1) the rod bipolar pathway (rod → rod bipolar → AII amacrine → On and Off cone bipolar terminals); (2) rod → (via gap junction) cone → cone bipolar cells; and (3) rod → a subset of Off cone bipolar cells. We identified stimulus conditions under which the rod bipolar pathway provided the dominant synaptic input to RGCs by using the mGluR6 agonist APB (Volgyi et al., 2004); responses in Off RGCs generated by the rod bipolar pathway (Figure 2A, gray) should be abolished by blockade of synaptic signaling between rods and rod bipolar cells with APB, while responses generated by stimuli that activate multiple pathways should be at least partially APB-insensitive.

APB (10–20 μM) almost completely eliminated spikes generated by stimuli producing ~2.5 Rh*/Rod/s and decreased, but did not eliminate, responses to higher-intensity stimuli (Figure 2B). Light-evoked EPSCs measured via whole-cell voltage-clamp recordings exhibited a similar sensitivity to APB; the EPSC variance in APB was <2% of that under control conditions for stimuli generating ~2.5 Rh*/Rod/s (Figure 2C). These experiments indicate that the rod bipolar pathway provides the dominant input to RGCs when light stimuli produce ≤2.5 Rh*/Rod/s.

Signals Carried by the Rod Bipolar Pathway Evoke Temporally Precise APs

To measure the temporal precision of APs generated by signals traversing the rod bipolar pathway, we recorded RGC responses to repeated presentations of a fluctuating full-field light stimulus that generated ~2.5 Rh*/Rod/s. Both 25% (Figure 3A$_1$; top) and 50% (Figure 3A$_1$; middle) contrast stimuli generated qualitatively reproducible bursts of APs. We quantified temporal precision using two complementary approaches.

To facilitate comparison with previous studies, we measured the standard deviation of the time of the first spike in selected bursts (Berry et al., 1997; Uzzell and Chichilnisky, 2004). Variability of the first spike time in

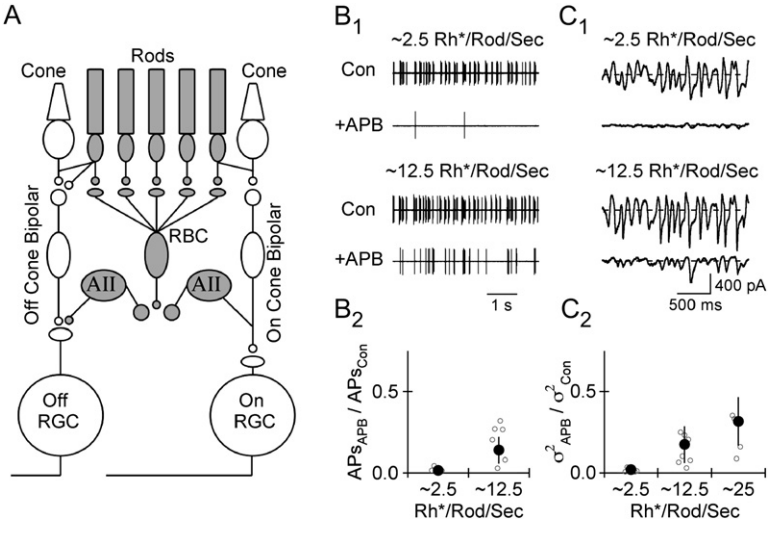

Figure 2. Stimuli Generating ≤2.5 Rh*/Rod/s Elicit Signals in RGCs via the Rod Bipolar Pathway

(A) Schematic of the retina. The unique elements of the rod bipolar pathway are highlighted in gray. AII, AII (rod) amacrine cell; RBC, rod bipolar cell.

(B$_1$) Cell-attached recording of spikes generated in an Off transient cell by light stimuli producing ~2.5 and ~12.5 Rh*/Rod/s in the absence (Con) and presence of the mGluR6 agonist L-APB (10 μM). (B$_2$) Ratio of the number of spikes in the presence and absence of APB.

(C$_1$) Whole-cell voltage-clamp (V_m= −70 mV) recording of the excitatory postsynaptic current (EPSC) in an Off transient cell evoked by light stimuli producing ~2.5 and ~12.5 Rh*/Rod/s under control conditions (Con) and in the presence of APB. (C$_2$) Ratio of synaptic current variance in the presence and absence of APB.

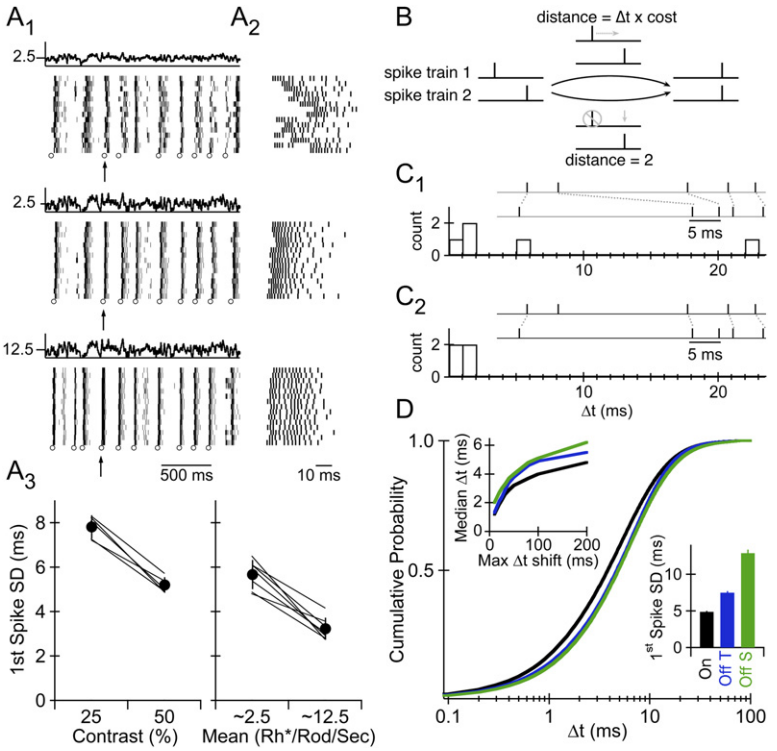

Figure 3. Input Provided by the Rod Bipolar Pathway Evokes Spikes with High Temporal Precision

(A_1) Light stimulus and raster plots of spike times during 15 consecutive trials for 25% (top) and 50% (middle) contrast stimuli producing 2.5 Rh*/Rod/s and 50% contrast stimuli producing 12.5 Rh*/Rod/s (bottom). Open circles at the base of each raster plot identify the bursts selected for analysis. (A_2) Expanded view of spike times in one burst across stimulus conditions. Burst time noted by arrow in (A_1). (A_3) Average standard deviation of the first spike time evoked by different mean and/or contrast stimuli in Off transient RGCs. Lines connect data recorded in the same cell. The average number of spikes in bursts selected for analysis was 10.1 ± 0.2, 8.9 ± 0.2, and 5.7 ± 0.2 in On, Off T, and Off S cells, respectively. The mean interspike interval of these spikes was 3.78 ± 0.04 ms, 4.54 ± 0.13 ms, and 4.51 ± 0.13 ms, respectively.

(B) Two operations in the spike distance metric enable a spike in one spike train to be paired with a spike in another spike train. The first operation (top) shifts (→) a spike in one spike train until it occurs at the same time as a spike in the other train, incurring a distance of (Δt × cost). The second operation (bottom) removes (⃠) a spike from one spike train and adds (↓) a spike at the appropriate time, incurring a distance of 2.

(C_1) When the cost of shifting spikes in time is low (0.02; max Δt shift = 100 ms), the total spike distance is minimized when all spikes are paired via shifting (despite the large Δt between some paired spikes). (C_2) When the cost of shifting spikes in time is high (0.2; max Δt shift = 10 ms), the spike distance is minimized by pairing spikes in one train with their nearest neighbor in the other spike train (in spite of the distance associated with removing/adding a spike). Note that the number of spikes paired via the shifting operation decreases as the cost of shifting spikes in time increases, and the Δt values for spikes paired via the shifting operation would not change if the distance associated with removing/replacing a spike was different.

(D) Cumulative probability distribution of Δt values for On (black), Off T (blue), and Off S (green) cells computed with cost = 0.025 (max Δt shift = 80 ms). In each case, error bars are observed by the line. The stimulus mean and contrast (~2.5 Rh*/Rod/s, 50%) was identical across cell types. (Top left inset) Relationship between median calculated Δt and the range over which spikes in one train could be shifted to match a spike in another train. The spike pairing algorithm removes/replaces a spike when Δt × cost ≥ 2; thus, max Δt shift = 2/cost. (Bottom right inset) Mean standard deviation of the first spike time in select bursts in the same cells.

Error bars, mean ± SEM.

bursts which (1) were preceded by ≥40 ms of quiescence and (2) contained a spike in ≥90% of trials (Figure 3A_1, open circles) decreased as the stimulus contrast and/or mean increased (Figure 3A_3). The standard deviation of the first spike time in different bursts ranged from 2 to 10 ms, a small fraction of the 300–500 ms duration of rod photoreceptor flash responses (Field and Rieke, 2002).

A fundamental problem with measures of spike timing precision is deciding which spikes should be compared across trials. The method used above circumvents this difficulty by considering the variability of a small number of easily identified spikes—i.e., the first spike in a subset of bursts. This approach is somewhat unsatisfactory, however, since the identified spikes represent <5% of the total spikes, and these spikes do not necessarily have a privileged role in the cortical readout of RGC activity.

The spike distance metric (Victor and Purpura, 1996) enables a complementary measure of spike timing precision without any ad hoc matching of spikes between responses or selection of relevant spikes. The metric defines the distance between a pair of spike responses by converting one response into the other through two operations: (1) shifting a spike in time (Figure 3B, top path); and (2) deleting a spike and/or adding a new one (Figure 3B, bottom path). The distance associated with shifting the spike in time is Δt × cost, where Δt is the time shift and cost is a variable. The distance associated with removing or adding a spike is defined as 1; the analysis described below is insensitive to the value of this parameter.

The decision of which operation to use is based on minimizing the distance—i.e., if Δt × cost < 2, the spike pairing algorithm inherent in the metric will shift one spike (top path in Figure 3B), whereas if Δt × cost > 2, a spike will be deleted/added (bottom path in Figure 3B). Thus, for a given cost, the spike distance metric identifies the spike pairings that minimize the total distance, and the temporal precision of those spikes that are aligned by shifting one spike in time can be quantified from histograms of the corresponding Δt values. When the cost of shifting spikes is low, the spike distance is minimized when nearly all spikes are paired via the shifting operation (Figure 3C_1). When the cost of shifting spikes in time is high, however, the spike distance is

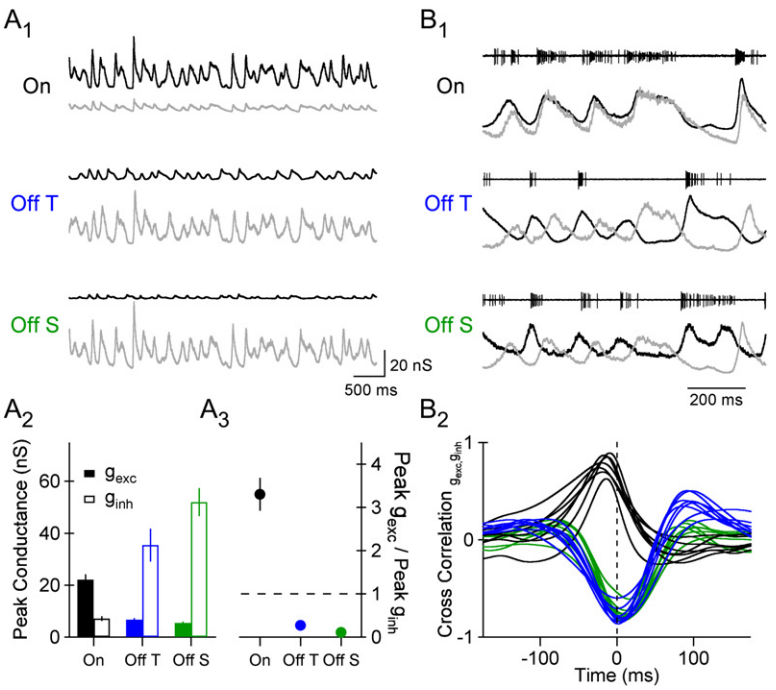

Figure 4. The Magnitude and Timing of Excitatory and Inhibitory Synaptic Input to On and Off RGCs Is Distinct

(A_1) A segment of the average excitatory (black) and inhibitory (gray) synaptic conductances generated in an On (top), Off T (middle), and Off S (bottom) cell by a fluctuating light stimulus that produced ~2.5 Rh*/Rod/s. (A_2) Mean peak excitatory (closed bars) and inhibitory (open bars) synaptic conductance for each RGC type (n = 7, 8, and 8). (A_3) Mean ratio of peak excitatory synaptic conductance to peak inhibitory synaptic conductance for each RGC type.

(B_1) Normalized excitatory (black) and inhibitory (gray) synaptic conductances from the corresponding cell in (A_1). Traces at the top of each panel are cell-attached recordings of spikes evoked by the same stimulus in the same cell. (B_2) Cross-correlation between the excitatory and inhibitory synaptic conductances for individual On (black), Off T (blue), and Off S (green) cells.

Error bars, mean ± SEM.

minimized by pairing some spikes via the remove/replace operation (Figure 3C_2).

We used this approach to characterize the temporal precision of light-evoked APs in three types of functionally identified mouse RGCs (see Figure 1). The distribution of Δt values derived from each pairwise comparison of recorded spike trains was calculated for a given cost; we varied the cost systematically such that the maximum Δt over which spikes could be paired via the shifting operation ranged from 10 to 200 ms. As expected, the median of the histogram of Δt values decreased as the range over which spikes could be shifted decreased (Figure 3D, top left inset), with a precipitous drop when the maximum Δt shift decreased below 50 ms. Thus, we compared the average cumulative distributions of Δt values derived from histograms in which spikes could be shifted by ≤80 ms (Figure 3D); to a reasonable approximation, this range of Δt values permits spikes within corresponding bursts to be paired via the shifting operation, but does not permit pairing of spikes across bursts. This procedure paired >85% of the spikes via the shift operation—i.e., this approach quantified the temporal precision of >85% of the light-evoked spikes in each RGC type.

The median Δt of spikes aligned via the spike distance metric was 4–5 ms (Figure 3D). Both this measure of temporal precision and the standard deviation of the first spike time (Figure 3D, bottom right inset) indicate that dim light stimuli generate APs with greater temporal precision in On cells than Off cells. Both measures indicate that input provided by the rod bipolar pathway generates temporally precise APs, despite the slow kinetics of the signals upon which these inputs are based.

Differences in Synaptic Input to On and Off RGCs

What excitatory and inhibitory synaptic conductances do dim light stimuli generate in each identified RGC type, and how does the integration of this synaptic input control the pattern and temporal precision of spike generation? To answer these questions we measured excitatory (g_{exc}) and inhibitory (g_{inh}) synaptic conductances evoked by fluctuating light stimuli that generated ~2.5 Rh*/Rod/s in each RGC type. As described below, the relative magnitude and timing of g_{exc} and g_{inh} varied substantially among RGC types. In the sections that follow, we determine the impact of these differences on spike generation.

We derived g_{exc} from synaptic currents measured at a holding potential of −75 mV, where there was little driving force for GABA/glycine receptor-mediated currents. Similarly, we derived g_{inh} from synaptic currents recorded at +10 mV, where there was little driving force for AMPA/KA/NMDA receptor-mediated currents. Synaptic currents measured at intermediate voltages were predicted accurately by summing the derived excitatory and inhibitory currents—i.e., the conductances weighted by the driving force (see Experimental Procedures); thus, g_{exc} and g_{inh} were isolated effectively.

Light-evoked synaptic conductances in all three RGC types were large—often exceeding 20 nS. The peak g_{exc} (22.2 ± 2.0 nS) in On cells was more than 3-fold larger than the peak g_{inh} (7.11 ± 0.9 nS; Figures 4A_1–4A_3). The opposite was true in Off transient and Off sustained cells, where g_{inh} was more than 5-fold larger than g_{exc} (Figures 4A_1–4A_3).

The temporal relationship between excitatory and inhibitory synaptic input also differed between On and Off cells. g_{exc} and g_{inh} had a similar time course in On cells, with inhibitory synaptic input slightly delayed relative to excitatory synaptic input (Figure 4B_1, top). For both Off transient and Off sustained cells, excitatory and inhibitory synaptic inputs were almost perfectly out of phase (Figure 4B_1, middle/bottom). We quantified the relative timing of excitatory and inhibitory synaptic

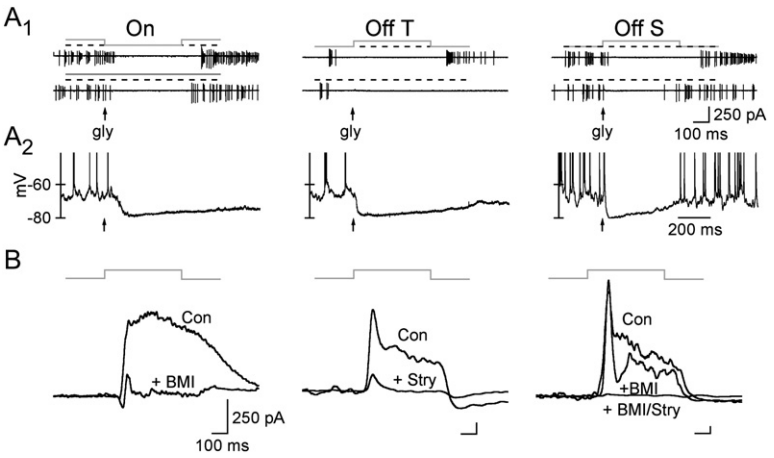

Figure 5. Reversal Potential and Postsynaptic Receptors Governing Inhibitory Synaptic Input

(A_1) Cell-attached recordings of APs following a step change in light intensity (top) or pressure application of glycine (100 μM, 10 ms pulse; bottom) to the soma of each RGC type. The gray line above each trace plots light intensity (relative to darkness, shown schematically as the dashed black line). (A_2) Effect of glycine on the voltage of each RGC type measured in perforated-patch recordings with gramicidin.

(B) Effect of the $GABA_A$ receptor antagonist bicuculline (BMI; 10 μM) and/or the glycine receptor antagonist strychnine (Stry; 1 μM) on light-evoked inhibitory postsynaptic current (IPSC; Vm = +10 mV) in On (left column), Off transient (middle column), and Off sustained (right column) RGCs.

inputs by computing the cross-correlation between the average g_{exc} and g_{inh} for individual RGCs. For On cells, the cross-correlation exhibited a strong positive peak at −16.4 ± 4.7 ms (n = 7; Figure 4B_2); the large negative peak of the cross-correlation between g_{exc} and g_{inh} in Off sustained and Off transient cells was offset slightly in the opposite direction (6.1 ± 4.4 ms). The positive correlation between g_{exc} and g_{inh}, and the delay of g_{inh} relative to g_{exc}, observed in On cells is expected for feedforward inhibition mediated by an amacrine cell that is itself postsynaptic to the On cone bipolar terminals that provide excitation to the RGC. The strong anticorrelation between g_{exc} and g_{inh} in Off cells, however, indicates that synaptic excitation and inhibition in the circuit providing input to Off RGCs operate in a push-pull fashion. We propose a basis for these timing differences in the Discussion.

Reversal Potential and Source of Inhibitory Synaptic Input to On and Off Cells

The effect of inhibitory conductances on spike generation depends on the reversal potential for inhibitory inputs. To test the possibility that inhibitory synaptic inputs are hyperpolarizing in some of the identified RGC types and shunting or depolarizing in others, we determined the effect of exogenous glycine via cell-attached and perforated-patch recordings. These experiments, unlike the experiments presented in Figure 4, permitted a cell to retain its normal complement of intracellular chloride. Brief pressure application of glycine to the soma transiently decreased the rate of AP generation in each RGC type (Figure 5A_1). Furthermore, application of glycine hyperpolarized each RGC type to near −80 mV in perforated-patch recordings using the Cl^- impermeant ionophore gramicidin (Figure 5A_2; Rhee et al., 1994; Ding and Perkel, 2002). Thus, glycine receptor-mediated conductances hyperpolarize each identified RGC, and differences in the reversal potential for inhibitory inputs are unlikely to produce substantial differences in synaptic integration between On and Off cells.

Although inhibitory input hyperpolarized each RGC type, the source of inhibition differed between On and Off cells. We determined the contributions of light-evoked GABAergic and glycinergic input by measuring the sensitivity of inhibitory synaptic currents measured at +10 mV to the $GABA_A$ receptor antagonist bicuculline and the glycine receptor antagonist strychnine at concentrations at which each drug acted relatively specifically (≤10 μM bicuculline, ≤1 μM strychnine; see Protti et al., 1997; Jonas et al., 1998). Inhibitory synaptic input to On cells was almost completely suppressed by bicuculline (Figure 5B) and only modestly affected by strychnine (data not shown), indicating that On cells receive predominantly GABAergic inhibition. Inhibitory input to Off transient and Off sustained cells was almost completely blocked by strychnine and relatively unaffected by bicuculline (Figure 5B), indicating that these RGC types receive predominantly glycinergic inhibition. We discuss the possible circuitry responsible for differences in synaptic inhibition in the Discussion.

Roles of Excitatory and Inhibitory Synaptic Conductances in Shaping Spike Output

Consistent with previous results (Pang et al., 2003; Zaghloul et al., 2003; Roska et al., 2006), On cells exhibited high firing rates when both excitatory and inhibitory synaptic conductances were active (Figure 4B_1, top), while Off cells exhibited high firing rates when excitatory synaptic conductances were active and inhibitory synaptic conductances were minimal (Figure 4B_1, middle/bottom). These differences suggest differences in the way synaptic conductances are integrated to control spike generation.

To test directly how differences in the amplitude and timing of excitatory and inhibitory synaptic inputs govern RGC spike generation, we injected light-evoked g_{exc} and/or g_{inh} using the conductance-clamp technique (Robinson and Kawai, 1993; Sharp et al., 1993). When the time-varying g_{exc} (or g_{inh}) was injected alone, the time-invariant mean of g_{inh} (or g_{exc}) was also injected to keep the cell's resting potential constant across conditions. In On cells, the pattern of spikes generated by g_{exc} alone was almost identical to that produced by g_{exc} and g_{inh} together; g_{inh} alone produced little modulation in spiking (Figure 6A_1, left column). In Off cells, however, somatic injection of g_{exc} alone generated unusually brief bursts of APs, while somatic injection of g_{inh} alone generated bursts of unusually low-frequency APs (Figure 6A_1, center/right columns) relative to APs evoked

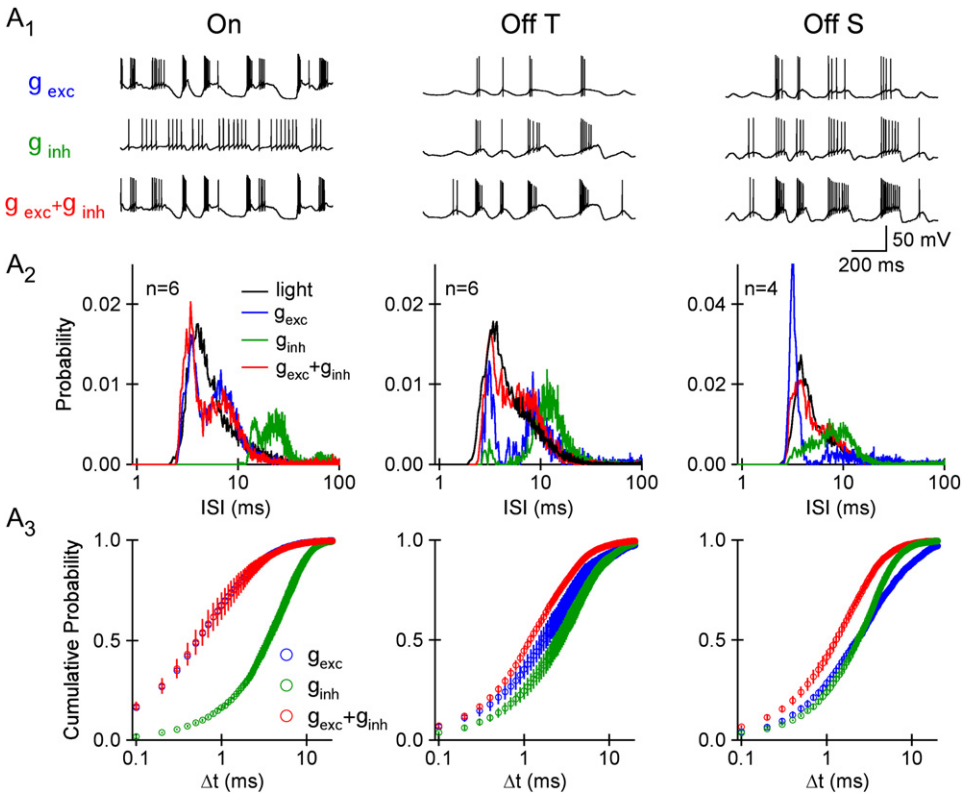

Figure 6. Synaptic Inhibition Shapes Response to Light Stimuli in Off, but Not On, RGCs

(A_1) Pattern of APs evoked by somatic injection of the cell-appropriate excitatory synaptic conductance (blue, top row), inhibitory synaptic conductance (green, middle row), or excitatory and inhibitory synaptic conductances (red, bottom row). (A_2) The distribution of interspike intervals (ISI) for spikes generated by excitatory, inhibitory, and excitatory + inhibitory synaptic conductance injection. The ISI distributions shown in black are from light-evoked spike trains recorded in the cell-attached configuration in the absence of synaptic receptor antagonists. The light-evoked ISI distribution and the synaptic conductance waveforms were measured for identical stimuli. For On cells, the mean squared error (MSE) between both the g_{exc} (blue) and g_{exc} + g_{inh} (red) ISI distribution and the light-evoked distribution was significantly less than that between the light-evoked distribution and the g_{inh} (green) distribution ($p < 0.02$). For Off cells, the MSE between the g_{exc} + g_{inh} and light-evoked ISI distributions was significantly less than that between either the g_{exc} or g_{inh} ISI distribution and the light-evoked distribution ($p < 0.015$, $n = 10$). (A_3) The cumulative probability distribution of Δt values for APs evoked by g_{exc} (blue), g_{inh} (green), and g_{exc} and g_{inh} (red). Conductance clamp experiments were performed in the presence of NBQX (5–10 μM), MK-801 (10 μM), and strychnine (10–20 μM). Strychnine at this concentration blocks both $GABA_A$ and glycine receptors (Jonas et al., 1998; Protti et al., 1997).
Error bars, mean ± SEM.

by g_{exc} and g_{inh} together. Thus, in Off cells, decreased inhibitory input permitted spike bursts while concomitant increased excitatory input shaped firing within the burst.

We used two approaches to quantify the impact of excitatory and inhibitory synaptic conductances on spike generation in On and Off cells. First, we calculated interspike interval (ISI) distributions for each cell type and each condition (Figure 6A_2). In On cells, the ISI distribution produced by injection of time-varying g_{exc} alone (Figure 6A_2, left column, blue) was indistinguishable from that generated by injecting time-varying g_{exc} and g_{inh} (red; $p > 0.4$; Kolmogorov-Smirnov test); both distributions were more similar to the ISI distribution of APs evoked directly by light stimuli (black) than the ISI distribution of APs evoked by g_{inh} alone (green). In Off cells, only the distribution of interspike intervals evoked by somatic injection of g_{exc} and g_{inh} together (red) resembled the distribution of interspike intervals for spikes evoked by fluctuating light stimuli (black).

Second, we used the spike pairing algorithm inherent in the spike distance metric (Victor and Purpura, 1996) to quantify the impact of g_{exc} and g_{inh} on the temporal precision of spike generation. Figure 6A_3 shows cumulative Δt distributions for each cell type and condition. In On cells the cumulative Δt distribution of APs generated by injecting g_{exc} alone was indistinguishable from that produced by g_{exc} and g_{inh} together ($p > 0.63$; Kolmogorov-Smirnov test). However, the temporal precision of APs evoked in Off transient cells by g_{exc} + g_{inh} exceeded that of APs evoked by g_{inh} alone ($p < 0.004$), while in Off sustained cells the precision of APs evoked by g_{exc} + g_{inh} was greater than spikes evoked by either g_{exc} ($p < 0.001$) or g_{inh} ($p < 0.003$) alone. Together, these results indicate that synaptic inhibition shapes the responses of Off cells much more than those of On cells, and that simultaneous decreases in synaptic inhibition and increases in synaptic excitation facilitate precise spike timing in Off RGCs.

Noise in Spike Generation Does Not Limit Temporal Precision of APs Evoked by Dim Light Stimuli

The temporal precision of RGC responses could be limited either by noise in a cell's synaptic inputs or by intrinsic noise in either dendritic processing or spike

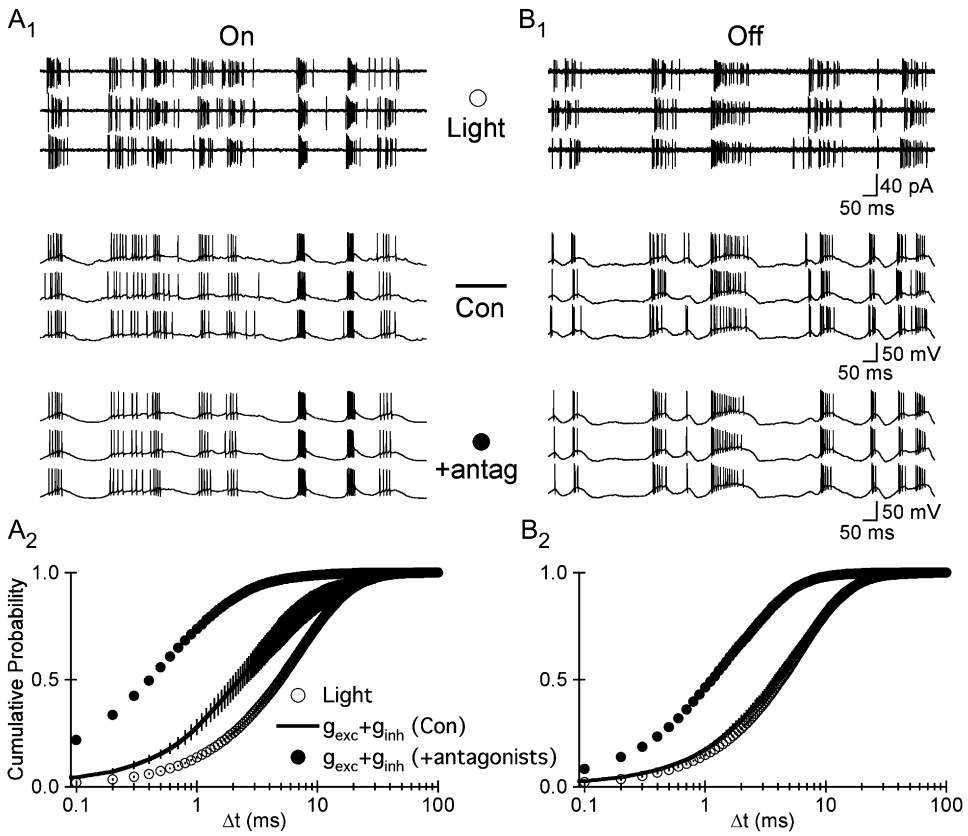

Figure 7. The Temporal Precision of APs Evoked by High-Contrast Stimuli Is Not Limited by Noise in Spike Generation

(A_1) (Top) Cell-attached recording of APs generated by an On cell in response to three consecutive trials of a fluctuating light stimulus that generated ~2.5 Rh*/Rod/s. (Middle) Three traces, from the same cell, of APs evoked in the dark by injecting the cell type-appropriate excitatory and inhibitory synaptic conductances. The synaptic conductances, g_{exc} and g_{inh}, and the APs shown in (A_1) were evoked by the same stimulus. (Bottom) Same as (A_1) (middle), except in the presence of NBQX (10 μM), MK-801 (10 μM), and strychnine (20 μM). (A_2) The cumulative probability distribution of Δt values for APs evoked by light stimuli (open circles), $g_{exc} + g_{inh}$ under control conditions (black line), and $g_{exc} + g_{inh}$ in the presence of glutamate, GABA, and glycine receptor antagonists (closed circles).

(B) Same as (A), except for Off cells.

Error bars, mean ± SEM.

generation. In pyramidal neurons, somatic injection of rapidly fluctuating current in the absence of synaptic input generates APs with high temporal precision (Mainen and Sejnowski, 1995), suggesting that spike generation contributes minimally to response variability. However, the mechanisms governing spike generation depend critically on the properties of synaptic input (Chance et al., 2002; Mitchell and Silver, 2003; Azouz and Gray, 2003; Shu et al., 2003; Zsiros and Hestrin, 2005), and the characteristics of physiological synaptic input are not known in most neuronal types. To determine the contribution of variability in spike generation under physiological conditions, we compared the temporal precision of spikes evoked directly by dim light stimuli with that of spikes elicited by somatic injection of light-evoked synaptic conductances.

Under control conditions, the pattern of APs evoked by fluctuating light stimuli closely resembled the pattern of APs generated by somatic injection of the average excitatory and inhibitory synaptic conductances evoked by the same stimulus in the same cell type (Figures 7A_1 and 7B_1). In On cells, the distribution of Δt values for APs evoked by $g_{exc} + g_{inh}$ in darkness was shifted to the left of values for light-evoked APs (Figure 7A_2). In Off cells, the median Δt of light- and conductance-evoked APs was indistinguishable ($p > 0.67$) under these conditions. Blocking glutamatergic, GABAergic, and glycinergic synaptic input had little effect on the overall pattern of APs evoked by somatic injection of synaptic conductances (Figures 7A_1 and 7B_1), but it substantially decreased the median Δt in both On ($p < 0.03$) and Off ($p < 0.001$) RGCs (Figures 7A_2 and 7B_2).

The low temporal variability of the conductance-evoked APs in the absence of synaptic input indicates that noise in the intrinsic mechanisms governing spike generation in the RGC types studied contributes little to the temporal variability of responses to this light stimulus. The increased variability of conductance-evoked APs in the presence of synaptic input indicates that background synaptic activity poses a significant limitation on temporal precision. Because the conductance-injection experiments of Figure 7 were performed in darkness, they likely underestimate the importance of background synaptic activity in On cells and overestimate its importance in Off cells. We return to this issue in the Discussion.

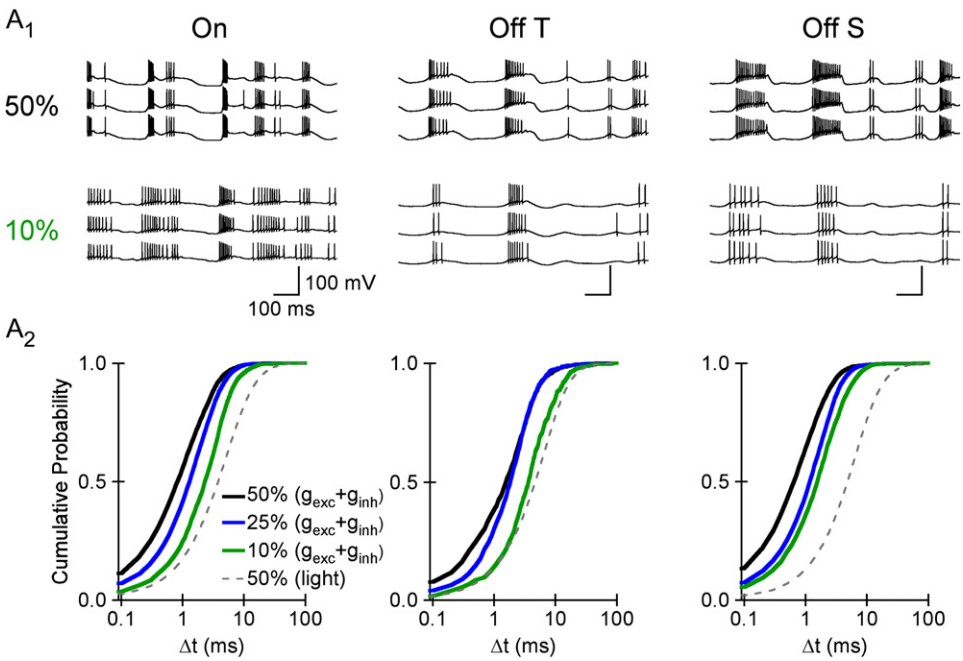

Figure 8. Spike Generation Does Not Limit Temporal Precision of APs Evoked by High- or Low-Contrast Stimuli

(A_1) Each panel shows three consecutive responses produced by somatic injection of the excitatory and inhibitory synaptic conductance waveforms evoked by 50% (top) or 10% (bottom) contrast stimuli for each RGC type. The 10% synaptic conductance waveforms were generated by convolving the synaptic conductances evoked by 50% contrast stimuli with the appropriate filter (see Figure S1B and Experimental Procedures). (A_2) The cumulative probability distribution of Δt values for spikes evoked by 50% (black), 25% (blue), and 10% (green) contrast conductance waveforms in an RGC of each type. For each cell type, the dashed gray line shows the average cumulative Δt distribution for spike responses evoked directly by 50% contrast light stimuli (from Figure 3). All conductance-clamp experiments in this figure were performed in the presence of NBQX (5–10 μM), MK-801 (10–20 μM), and strychnine (10–20 μM).

The temporal variability of light-evoked APs increases as stimulus contrast decreases (Figure 3A_3; Berry et al., 1997; Uzzell and Chichilnisky, 2004), and noise in the mechanisms governing spike generation may limit detection of low-contrast stimuli (Dhingra and Smith, 2004). Could intrinsic noise contribute to variability when light stimuli produce smaller and slower changes in the membrane potential? To answer this question we first compared the amplitude and kinetics of light-evoked excitatory and inhibitory synaptic conductances for 10%, 25%, and 50% contrast stimuli. As expected, lower-contrast stimuli produced smaller and more slowly varying changes in g_{exc} and g_{inh} in each RGC type (see Figure S1 in the Supplemental Data).

To test directly whether variability in spike generation limited the precision of responses evoked by lower-contrast stimuli, we compared the temporal precision of APs evoked by somatic injection of synaptic conductances corresponding to high-, medium-, and low-contrast light stimuli in the presence of glutamate, GABA, and glycine receptor antagonists. The overall pattern of APs generated by high (50%) and low (10%) synaptic conductances in a given cell was similar (Figure 8A_1). Consistent with results from cell-attached recordings of light-evoked AP generation, the low-contrast excitatory and inhibitory synaptic conductances generated more APs in On cells, and fewer APs in Off cells, compared with the high-contrast excitatory and inhibitory synaptic conductances (Figure 8A_1).

The temporal precision of APs generated by the injected synaptic conductances decreased as the contrast of the stimulus evoking the synaptic conductances decreased (Figure 8A_2). However, the temporal precision of APs evoked by even the lowest (10%) contrast synaptic conductances was greater than that of spikes evoked directly by high-contrast light stimuli (Figure 8A_2, gray dashed lines) in each On, Off transient, and Off sustained RGC examined (n = 4, 3, and 3, respectively). These results show that noise in spike generation does not limit the temporal precision of APs evoked by high- or low-contrast stimuli with a mean intensity of ~2.5 Rh*/Rod/s in each type of identified RGC.

Temporal Variability of Light-Evoked APs Reflects Variability in Network Input

The results presented thus far indicate that variability in the mechanisms governing spike generation does not contribute significantly to the variability of light-evoked activity in each identified RGC type. Two observations suggest that active dendritic properties are not required to generate precisely timed APs: (1) somatic injection of light-evoked synaptic conductances closely mimicked the pattern and temporal precision of responses evoked by light stimuli; and (2) hyperpolarizing RGCs in current clamp did not reveal any light-evoked "spikelets" or other signatures of active dendritic processing (e.g., Oesch et al., 2005; data not shown). Therefore, we tested directly the possibility that trial-to-trial variability in synaptic input to RGCs (Figure 9A) limits the temporal precision of light-evoked AP generation.

In these experiments we injected individual, rather than averaged, synaptic conductance waveforms recorded

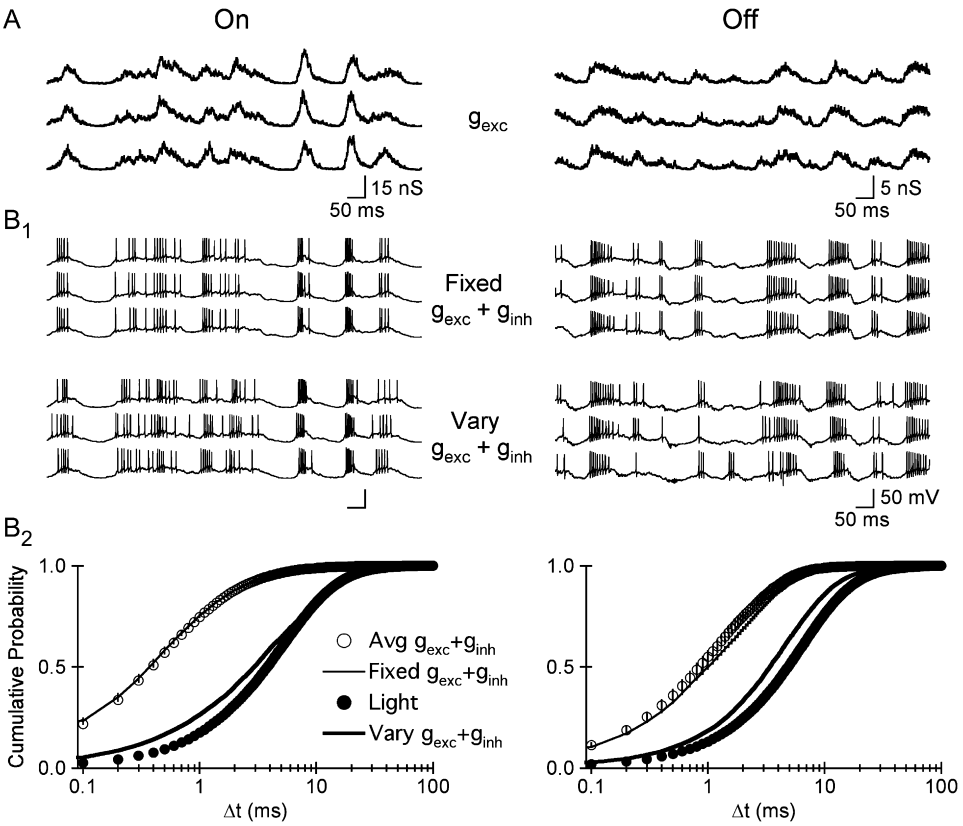

Figure 9. Variability in Synaptic Input Limits Spike Timing Precision

(A) g_{exc} evoked in an On (left) and Off S (right) RGC on three consecutive trials by dim fluctuating light stimuli that generated ~2.5 Rh*/Rod/s. (B_1) (Top) APs evoked in three separate trials by the same pair of excitatory and inhibitory synaptic conductance waveforms. (Bottom) APs evoked on three separate trials in the same cell by three unique pairs of excitatory and inhibitory synaptic conductance waveforms. (B_2) The cumulative probability distribution of Δt values for APs evoked by repeatedly injecting the same pair of individual excitatory and inhibitory waveforms (thin line), repeatedly injecting the average excitatory and inhibitory synaptic conductance (open circles), injecting random pairings of individual excitatory and inhibitory synaptic conductance waveforms (thick line), and light stimuli (closed circles; from Figure 3). All conductance-clamp experiments were performed in the presence of AMPA/KA, NMDA, glycine, and $GABA_A$ receptor antagonists.
Error bars, mean ± SEM.

on consecutive trials from a single cell of each type. We alternated trials using the same pair of measured individual excitatory and inhibitory synaptic conductances (Figure 9B, Fixed g_{exc} + g_{inh}) with trials where we injected single randomly selected excitatory and inhibitory synaptic conductance waveforms recorded from the same cell (Figure 9B, Vary g_{exc} + g_{inh}). These experiments were performed with glutamatergic, GABAergic, and glycinergic synaptic input blocked, but variability from both background and light-evoked synaptic input contributed to the individual measured conductance waveforms. These experiments therefore determined the impact of trial-to-trial variability in a cell's synaptic inputs on the temporal precision of AP generation.

As expected, the median Δt of spikes evoked by repeated injection of the same pair of individual conductance waveforms (Figure 9B_2, thin line) and the average synaptic conductances (open circles) was indistinguishable in both On ($p > 0.77$; $n = 5$) and Off ($p > 0.78$, $n = 5$) cells. However, the temporal precision of APs evoked by individual conductance waveforms that varied from trial to trial (Figure 9B_2; thick black line) was reduced, nearly mimicking the precision of spikes evoked directly by light stimuli in separate experiments (closed circles, from Figure 3). These results indicate that the measured trial-to-trial variability in synaptic input provided by the rod bipolar pathway underlies the trial-to-trial variability of light-evoked AP generation in each identified RGC type.

Discussion

Previous attempts to understand the processes governing variability of stimulus-evoked responses fall into two broad categories. The first approach has been to infer the pattern and variability of synaptic input, and the way in which this synaptic input is integrated, from the responses to sensory stimuli (Gabernet et al., 2005; Pillow et al., 2005; Wehr and Zador, 2003; Azouz and Gray, 2003; Keat et al., 2001). The second approach has been to identify synaptic and cellular mechanisms that facilitate the temporal precision of spikes evoked by electrical stimulation of brain slices (Pouille and Scanziani, 2001; Galarreta and Hestrin, 2001; Blitz and Regehr, 2005; Bacci and Huguenard, 2006). We have used the mammalian retina to examine in parallel the temporal precision of light-evoked APs and the synaptic and cellular mechanisms governing this precision. This

approach enabled us to (1) uncover a profound difference in the way excitatory and inhibitory synaptic input governs light-evoked activity in On and Off retinal ganglion cells, and (2) demonstrate directly that the temporal variability of light-evoked AP generation is a consequence of variability in synaptic input.

Amplitude, Timing, and Origin of RGC Synaptic Conductances

The neural circuits that govern light-evoked AP generation are often too complicated, too intractable, or too incompletely understood to test directly the contribution of stimulus, network, and/or intrinsic variability to response variability. We circumvented this problem by identifying lighting conditions under which the vast majority of synaptic input to three functionally-identified types of mouse RGCs was provided by a relatively well-characterized circuit in the retina—the rod bipolar pathway. These stimuli generated reproducible and temporally precise patterns of APs in each RGC type. However, dim light stimuli generated much larger excitatory than inhibitory synaptic input in On cells and much larger inhibitory than excitatory synaptic input in Off cells. Furthermore, the relative timing of light-evoked excitatory and inhibitory synaptic input to On and Off cells differed profoundly; g_{exc} and g_{inh} were highly correlated in On cells, and almost perfectly anticorrelated in Off cells. These results are consistent with recent data suggesting that light stimuli govern AP generation in On and Off alpha and parasol RGCs via unique neural circuits (Chichilnisky and Kalmar, 2002; Pang et al., 2003; Zaghloul et al., 2003; Roska et al., 2006).

What is the basis for these differences? Anatomical evidence suggests that AII amacrine cells form glycinergic synaptic contacts with Off cone bipolar synaptic terminals and the dendrites of Off, but not On, ganglion cells in the mammalian retina (Famiglietti and Kolb, 1975; Kolb, 1979; Strettoi et al., 1992; Owczarzak and Pourcho, 1999). Indeed, inhibitory input to Off sustained and Off transient RGCs, but not On RGCs, was predominantly glycinergic. These observations suggest that the large light-evoked inhibitory synaptic input to both Off transient and Off sustained RGCs is mediated by AII amacrine cells. This interpretation is consistent with the strong correlation between g_{inh} in Off transient and Off sustained cells (0.85 ± 0.08) and the temporal relationship between g_{exc} and g_{inh} in Off RGCs; depolarizing an AII amacrine cell would cause an increase in direct inhibitory input to Off RGCs and a concomitant decrease in the glutamatergic input provided by synaptically coupled Off cone bipolars. This interpretation is also consistent with the observation that light-evoked g_{exc} in On cells was strongly correlated with g_{inh} in Off cells (peak = 0.875 ± 0.08; see Figure 3A_1), although we cannot exclude the possibility that synaptic inhibition in Off RGCs is provided by a glycinergic amacrine cell that is postsynaptic to On cone bipolar cells.

Quantification of Temporal Precision

We employed several complementary approaches to describe the temporal precision of RGC spike generation. The first approach, based on previous studies (Berry et al., 1997; Uzzell and Chichilnisky, 2004), characterized the standard deviation of the time at which the first spike in a subset of light-evoked bursts occurred. This method provides an intuitive and easily quantifiable measure of temporal precision, but it assumes that variability of the first spike is either representative, or more important, than that of other spikes. The second approach used the spike pairing algorithm inherent in the spike distance metric (Victor and Purpura, 1996). This approach offers several distinct advantages. First, the algorithm quantifies the precision of the majority (85%–95%) of spikes evoked by dim light stimuli. Second, the rules governing how spikes are paired can be controlled in an explicit (and parametric) manner, making it clear how details of the pairing influence conclusions.

Both measures indicated that signals traversing the rod bipolar pathway evoked spikes in each of the three identified RGC types with a temporal precision of 2–10 ms. This precision is about 50-fold greater than the $\sim$300 ms integration time of the rod photoreceptor responses, and it is similar to the precision of APs evoked by light stimuli $\geq$1000 times brighter (Berry et al., 1997; Uzzell and Chichilnisky, 2004). Thus, the circuitry of the rod bipolar pathway exploits convergence and the low noise of the rod responses to generate temporally precise responses from the relatively sluggish rod signals.

Using Light-Evoked Synaptic Conductances to Control AP Generation

Previous attempts to understand the role of direct inhibitory synaptic input onto ganglion cells have compared the response to light stimuli in the absence and presence of GABA and/or glycine receptor antagonists (e.g., Roska et al., 1998; Olveczky et al., 2003; Ishikane et al., 2005). This approach blocks GABA and glycine receptors on ganglion cells as well as on the cells presynaptic to ganglion cells (reviewed in Wassle et al., 1998; Grunert, 2000), making interpretation of effects difficult. We used somatic injection of light-evoked synaptic conductances to test how excitatory and inhibitory synaptic input governs the pattern and temporal precision of RGC spike generation. This strategy enabled us to manipulate excitatory and inhibitory synaptic input independently. We found that the pattern and temporal precision of spikes evoked by somatic injection of g_{exc} alone did not differ substantially from the pattern and temporal precision elicited by g_{exc} and g_{inh} together in On RGCs. In Off sustained and Off transient RGCs, however, only the pattern of spikes generated by g_{exc} and g_{inh} together resembled that evoked by light stimuli, and the temporal precision of APs generated by g_{exc} + g_{inh} was greater than that of APs evoked by either g_{exc} or g_{inh} alone. These results indicate that On and Off cells employ unique strategies to facilitate spike timing precision. Precise AP generation in On cells is produced by large changes in excitatory synaptic conductances. Precise AP generation in Off cells is facilitated by dynamic changes in excitatory and inhibitory synaptic conductances, with a decrease in inhibition permitting the cell to generate a burst of spikes, and a concomitant increase in excitation shaping the pattern of spikes during the burst.

The ability of responses generated by somatic injection of light-evoked synaptic conductances to mimic light-evoked responses depends critically on (at least)

two assumptions: (1) voltage-dependent properties of the dendrites do not significantly alter the impact of the conductance at the soma, and (2) we measure the synaptic conductances that are most critical for governing the cell's output. We looked for, but did not find, light-evoked spikelets or other signatures of regenerative dendritic processes like those observed recently in direction-selective RGCs (Oesch et al., 2005). The light-evoked excitatory synaptic conductances we recorded and injected, however, may have lacked an NMDA receptor-mediated component; at −75 mV, where we measured light-evoked excitatory synaptic currents, NMDA receptors are generally blocked by extracellular Mg^{2+} (Mayer et al., 1984; Nowak et al., 1984). In the presence of GABA and glycine receptor antagonists, EPSCs evoked by light and/or electrical stimuli are reduced by NMDA receptor antagonists (Diamond and Copenhagen, 1993, 1995; Hensley et al., 1993; Matsui et al., 1998), demonstrating conclusively that synaptically released glutamate can evoke NMDA receptor-mediated conductances in RGCs. It is unclear, however, to what extent these conductances contribute under physiological conditions. We found that light-evoked synaptic currents measured at −30 mV were predicted accurately by the weighted sum of synaptic conductances recorded at −75 mV (g_{exc}) and +10 mV (g_{inh}; see Experimental Procedures). This suggests that NMDA receptor-mediated conductances in the three identified RGC types we studied contribute very little and/or are accurately reflected by synaptic currents measured at −75 mV.

Variability of RGC Spike Generation Reflects Variability of Synaptic Input

The effect of network and intrinsic noise on the precision of spike generation has caused considerable debate and controversy for more than a decade (Softky and Koch, 1993; Shadlen and Newsome, 1994). In the absence of network noise, somatic injection of fluctuating current evokes APs that exhibit high temporal precision in cortical pyramidal neurons (Mainen and Sejnowski, 1995), suggesting that the variability of light-evoked responses reflects variability in the synaptic input a cell receives. However, the intrinsic mechanisms governing spike generation and synaptic integration can change as properties of the input change (Chance et al., 2002; Mitchell and Silver, 2003; Azouz and Gray, 2003; Shu et al., 2003; Zsiros and Hestrin, 2005), and neither the baseline nor stimulus-evoked synaptic input to most neurons is well understood. We found that APs generated by somatic injection of light-evoked synaptic conductances in the absence of synaptic input had a much higher precision than light-evoked APs. This result held true for injected synaptic conductances elicited by high- (50%) or low- (10%) contrast stimuli. Thus, noise in spike generation does not limit temporal precision for the stimuli tested in any of the three identified RGC types studied.

What noise sources govern the reproducibility of light-evoked RGC responses? Temporal precision was similar for APs evoked directly by light stimuli and for APs evoked by somatic injection of measured synaptic conductances that varied from trial to trial. This similarity indicates that the noise governing the temporal precision of light-evoked APs is a feature of the network through which light-evoked signals propagate. Our results, however, do not determine the relative contribution of variability in synaptic inputs evoked by constant and time-varying light stimuli with the same mean intensity. The temporal precision of APs evoked in darkness by somatic injection of measured synaptic conductances suffered in the absence of synaptic receptor antagonists (Figure 5), indicating that background synaptic activity can influence the temporal precision of AP generation. However, examining the effect of synaptic input in the dark on APs evoked by somatic injection of synaptic conductances likely resulted in an underestimation of the impact of background synaptic variability on APs evoked in On cells, since synaptic input to these cells increases as light intensity increases. It is similarly difficult to interpret the influence of background input on Off cells because variability in their synaptic input likely decreases as light intensity increases.

We have focused on conditions under which signals traversing the rod bipolar pathway dominate. Examining properties of light-evoked responses in the cells presynaptic to RGCs in this circuit will enable us to identify and manipulate the processes that facilitate reproducible and temporally precise responses to dim light stimuli in the early visual system.

Experimental Procedures

Tissue Preparation

Mice (c57/BL6, 6–8 weeks old) were dark adapted overnight and sacrificed according to protocols approved by the Administrative Panel on Laboratory Animal Care at the University of Washington. After hemisecting each eye, we removed the vitreous mechanically and stored the eyecup in a light-tight container in warm (~32°C), bicarbonate-buffered Ames Solution (Sigma-Aldrich, St. Louis) equilibrated with 5% CO_2/95% O_2. These and all subsequent procedures were carried out under infrared light (>900 nm) to keep the retina dark adapted.

All experiments were performed in a flat mount preparation of the retina. We cut a wedge from the eye cup and gently separated the retina from the retinal pigment epithelium. We placed the isolated retina ganglion cell-side up on a small piece of filter paper or nylon mesh and transferred it into a recording chamber. The retina was secured by nylon wires stretched across a platinum ring and perfused with warm (30°C–34°C) equilibrated Ames solution flowing at 6–8 mL/min.

Light Stimuli and Data Collection

Light from a light-emitting diode (LED; peak output = 470 nm) was delivered to the recording chamber via a fiber optic cable. The spatially uniform light stimulus illuminated a circular area 0.65 mm in diameter, centered on the recorded cell. Calibrated photon fluxes at the preparation were converted to photoisomerization rates (Rh*/Rod/s) from the spectral output of the LED, the absorption spectrum of rhodopsin, and an assumed collecting area per rod of 0.5 μm^2. Most experiments used repeated presentations of a full-field stimulus with a temporal trajectory drawn from a Gaussian distribution (bandwidth 0–60 Hz). The contrast of this stimulus was defined as the standard deviation divided by the mean.

We used several complementary approaches to record RGC light-evoked signals. We made cell-attached recordings with glass pipettes (4–6 MΩ) filled with Ames solution to record the pattern of light-evoked spikes without disrupting the internal composition of RGCs (Figure 1A). To characterize light-evoked excitatory and inhibitory RGC synaptic input, we performed whole-cell voltage-clamp recordings (Figure 1B) with pipettes filled with an internal solution containing 105 mM $CsCH_3SO_3$, 10 mM TEA-Cl, 20 mM HEPES, 10 mM EGTA, 5 mM Mg-ATP, 0.5 mM Tris-GTP, and 2 mM QX-314 (pH ~7.3 with CsOH, ~280 mOsm). Series resistance for

voltage-clamp recordings (~15 MΩ) was compensated electronically by ≥75%. We corrected for the ~10 mV junction potential offline.

The calculated chloride reversal potential with this internal solution is −77 mV; thus, the absolute driving force for excitatory postsynaptic currents at the chloride reversal potential is equal to that for the inhibitory postsynaptic currents recorded at the reversal potential for excitatory postsynaptic current (~+10 mV). To determine whether excitatory (and inhibitory) postsynaptic currents were isolated effectively at −75 (or +10 mV), we computed the mean squared error (MSE) between the mean response recorded at −30 mV and (1) individual recorded trials and (2) the response predicted from the sum of $g_{exc} \times (-0.045) + g_{inh} \times (0.03)$. The absolute value of the driving force for inhibitory synaptic conductances was assumed to be 30 mV (rather than 40) because of the likely voltage error due to uncompensated series resistance. The MSE between the mean and individual measured responses at −30 mV was greater than that between the mean and predicted responses in 8/9 cells.

To measure the native chloride reversal potential, we made perforated-patch recordings with a solution containing the Cl^- impermeable ionophore gramicidin. For these experiments the patch pipette contained 120 mM CsCl, 10 mM TEA-Cl, 3 mM Mg-ATP, 0.3 Tris-GTP, and 0.25–0.5 μg/mL gramicidin (pH ~7.3, ~280 mOsm). Glycine (100 μM) was applied to the soma via a Picospritzer (Intracel, Herts, UK). For whole-cell current- and conductance-clamp recordings, we used an internal solution containing 125 mM K Aspartate, 10 mM KCl, 1 mM $MgCL_2$, 10 mM HEPES, 5 mM NMDG-EDTA, 0.5 mM $CaCl_2$, 10 mM phosphocreatine, 4 mM Mg-ATP, and 0.5 Tris-GTP (pH ~7.2 with KOH, ~280 mOsm).

Signals were amplified with an Axoclamp 200B (Axon Instruments; Foster City, CA) amplifier, filtered at 3 kHz (8 pole Bessel low-pass), and sampled at 10 kHz (ITC16 interface, Instrutech Corporation, Port Washington, NY). The current injected during conductance-clamp experiments was calculated from the measured cell voltage, the reversal potentials for excitatory (0 mV) and inhibitory (−80 mV) inputs, and the measured conductance waveforms. The feedback between measured voltage and injected current operated on each voltage sample—i.e., at 10 kHz. Conductance waveforms measured from different cells of the same type were very similar (mean peak cross-correlation >0.88 and >0.82 for excitatory and inhibitory inputs, respectively). Thus, the conductance-clamp experiments used conductance waveforms from one example cell of each type. Unless otherwise noted, conductance-clamp experiments were performed in the presence of 5–10 μM NBQX, 10–20 μM MK-801, and 10–20 μM strychnine to block AMPA/Kainate, NMDA, and GABA/glycine receptors, respectively.

Data Analysis

All analyses were performed using procedures written in MATLAB (The MathWorks, Natick, MA). We identified spikes recorded in both cell-attached and whole-cell recording configurations with a threshold crossing algorithm; the time at which each identified event peaked was defined as the spike time. We predominantly used the spike pairing algorithm inherent in the spike distance metric (Victor and Purpura, 1996) to measure the temporal precision of light-evoked APs. The spike distance metric creates a matrix with the number of rows and columns equal to the number of spikes in spike trains $S_A + 1$ and $S_B + 1$, respectively. For a given cost of shifting spikes in time, each element in the matrix is filled according to the following equation:

$$SCR_{i,j} = \min\{SCR_{i-1,j} + 1, SCR_{i,j-1} + 1, SCR_{i-1,j-1} + cost \times (|S_A(i-1) - S_B(j-1)|)\}$$

The value in the last row and last column of this "scr" matrix represents the total spike distance.

We calculated from the scr matrix a corresponding "subtraction" matrix where each element reflects the difference between the real scr matrix and a scr matrix in which all spikes were paired via the remove/replace operation $[subtraction_{i,j} = SCR_{i,j} - ((i-1) + (j-1))]$. The value in each element of this subtraction matrix therefore represents the savings in spike distance that has accumulated by pairing all spikes prior to $S_A(i-1)$ and $S_B(j-1)$ via the shifting operation. Stepping up, left, or up and left through the subtraction matrix along the path that provides the most savings corresponds to tracing backward through the same unique path in the scr matrix that minimized the spike distance. Lateral and vertical movements through the subtraction (or scr) matrix correspond to pairing different spikes in S_B with the same spike in S_A and different spikes in S_A with the same spike in S_B, respectively.

Because a single spike in spike train S_A can only be paired with a single spike in spike train S_B, the unique spike pairings that minimize the total spike distance must be at least one row above and one column to the left of the last identified spike pair. Thus, starting in the element in the last row/column of the subtraction matrix [$subtraction_{i,j}$], and for each subsequent step, one determines whether the absolute value of the element to the left or above is greater. If, for example, the value of the element above [$subtraction_{i,j-1}$] is greater than that to the left [$subtraction_{i-1,j}$], and the absolute value of the element above is less than the current element, one pairs spikes $S_A(i-1)$ and $S_B(j-1)$ and determines the difference in time between them (Δt). In this case, $S_A(i-1)$ and $S_B(j-1)$ are paired because this pairing results in a smaller spike distance than pairing spikes $S_A(i-1)$ and $S_B(j-2)$.

If however the value of the element above is greater than that to the left of the current element, but is not different from the value of the current element, one simply steps vertically to that element without identifying $S_A(i-1)$ and $S_B(j-1)$ as a pair. This is because the algorithm that computes the spike distance metric pairs spikes from the beginning of the spike trains, corresponding to the top left corner of the scr matrix, to the end of the spike trains, corresponding to the bottom right corner of the scr matrix. Therefore, while traversing a row or column in the subtraction matrix where the value of the elements remains the same, the appropriate (unique) spike pairing between spike S_A and S_B corresponds to the coordinates of the element furthest to the left/top of the row/column.

If the value of the elements in the subtraction matrix above [$subtraction_{i,j-1}$] and to the left [$subtraction_{i-1,j}$] of the current element [$subtraction_{i,j}$] have the same value, one moves diagonally up and to the left. As with any purely vertical or horizontal movement, one only recognizes the spike pair $S_A(i-1)$, $S_B(j-1)$ if the value of the current element [$subtraction_{i,j}$] is different from the value of the next element [$subtraction_{i-1,j-1}$]. If the value of these two elements in the subtraction matrix were equal, the spikes $S_A(i-1)$ and $S_B(j-1)$ were paired via the remove/replace operation.

We calculated the cross-correlation between average g_{exc} and g_{inh} in a given cell according to the following equation:

$$C(n) = \frac{\sum_{i=1}^{N} x_i y_{i-n}/N}{\sqrt{\frac{(x_i - x_i)}{N} \times \frac{(y_{i-n} - y_{i-n})}{N}}}$$

The Fourier transform of the linear filter between each response evoked by a 50% contrast stimulus and each response evoked by a 25% or 10% stimulus is given by:

$$F = \frac{<y \times x'>}{<x \times x'>}$$

where y is the Fourier transform of a response evoked by 25% or 10% stimuli, x is the Fourier transform of a response evoked by 50% contrast stimuli, and x' is the conjugate of x. We then averaged across all filters for a given cell and condition. The peak of the cross-correlation between individual measured trials and the mean was smaller than that between the mean response and each predicted response in every experiment examined, indicating that the predicted responses were indistinguishable from measured responses obtained on individual trials. We used the filters constructed from one On cell to transform the 50% conductance waveforms (recorded from another cell) so that the average 50% excitatory and inhibitory synaptic conductance waveforms were identical across experiments.

Statistical significance was tested with the Student's t test unless noted otherwise. Data are presented as mean ± SEM throughout the text and figures.

Supplemental Data

The Supplemental Data for this article can be found online at http://www.neuron.org/cgi/content/full/52/3/511/DC1/.

Acknowledgments

We thank Abby Person, David Perkel, Kevin Briggman, Barry Wark, Greg Field, Thuy Doan, and Felice Dunn for detailed comments on the manuscript, and Eric Martinson and Paul Newman for excellent technical assistance. Support was provided by HHMI and the NIH (EY-11850).

Received: June 2, 2006
Revised: August 7, 2006
Accepted: September 7, 2006
Published: November 8, 2006

References

Arabzadeh, E., Zorzin, E., and Diamond, M.E. (2005). Neuronal encoding of texture in the whisker sensory pathway. PLoS Biol. *3*, e17. 10.1371/journal.pbio.0030017.

Azouz, R., and Gray, C.M. (2003). Adaptive coincidence detection and dynamic gain control in visual cortical neurons in vivo. Neuron *37*, 513–523.

Bacci, A., and Huguenard, J.R. (2006). Enhancement of spike-timing precision by autaptic transmission in neocortical interneurons. Neuron *49*, 119–130.

Beierlein, M., Gibson, J.R., and Connors, B.W. (2000). A network of electrically coupled interneurons drives synchronized inhibition in neocortex. Nat. Neurosci. *3*, 904–910.

Berry, M.J., Warland, D.K., and Meister, M. (1997). The structure and precision of retinal spike trains. Proc. Natl. Acad. Sci. USA *94*, 5411–5416.

Blitz, D.M., and Regehr, W.G. (2005). Timing and Specificity of feed-forward inhibition within the LGN. Neuron *45*, 917–928.

Bloomfield, S.A., and Dacheux, R.F. (2001). Rod vision: pathways and processing in the mammalian retina. Prog. Retin. Eye Res. *20*, 351–384.

Buracas, G.T., and Albright, T.D. (1999). Gauging sensory representations in the brain. Trends Neurosci. *22*, 303–309.

Buracas, G.T., Zador, A.M., DeWeese, M.R., and Albright, T.D. (1998). Efficient discrimination of temporal patterns by motion-sensitive neurons in primate visual cortex. Neuron *20*, 959–969.

Carr, C.E. (1993). Processing of temporal information in the brain. Annu. Rev. Neurosci. *16*, 223–243.

Chance, F.S., Abbott, L.F., and Reyes, A.D. (2002). Gain modulation from background synaptic input. Neuron *35*, 773–782.

Chichilnisky, E.J., and Kalmar, R.S. (2002). Functional asymmetries in ON and OFF ganglion cells of primate retina. J. Neurosci. *22*, 2737–2747.

DeWeese, M.R., Wehr, M., and Zador, A.M. (2003). Binary spiking in auditory cortex. J. Neurosci. *23*, 7940–7949.

Dhingra, N.K., and Smith, R.G. (2004). Spike generator limits efficiency of information transfer in a retinal ganglion cell. J. Neurosci. *24*, 2914–2922.

Diamond, J.S., and Copenhagen, D.R. (1993). The contribution of NMDA and non-NMDA receptors to the light-evoked input-output characteristics of retinal ganglion cells. Neuron *11*, 725–738.

Diamond, J.S., and Copenhagen, D.R. (1995). The relationship between light-evoked synaptic excitation and spiking behaviour of salamander retinal ganglion cells. J. Physiol. *487*, 711–725.

Ding, L., and Perkel, D.J. (2002). Dopamine modulates excitability of spiny neurons in the avian basal ganglia. J. Neurosci. *22*, 5210–5218.

Famiglietti, E.V.J., and Kolb, H. (1975). A bistratified amacrine cell and synaptic circuitry in the inner plexiform layer of the retina. Brain Res. *84*, 293–300.

Field, G.D., and Rieke, F. (2002). Nonlinear signal transfer from mouse rods to bipolar cells and implications for visual sensitivity. Neuron *34*, 773–785.

Field, G.D., Sampath, A.P., and Rieke, F. (2005). Retinal processing near absolute threshold: from behavior to mechanism. Annu. Rev. Physiol. *67*, 491–514.

Gabernet, L., Jadhav, S.P., Feldman, D.E., Carandini, M., and Scanziani, M. (2005). Somatosensory integration controlled by dynamic thalamocortical feed-forward inhibition. Neuron *48*, 315–327.

Galarreta, M., and Hestrin, S. (2001). Spike transmission and synchrony detection in networks of GABAergic interneurons. Science *292*, 2295–2299.

Grunert, U. (2000). Distribution of GABA and glycine receptors on bipolar and ganglion cells in the mammalian retina. Microsc. Res. Tech. *50*, 130–140.

Hensley, S.H., Yang, X.L., and Wu, S.M. (1993). Identification of glutamate receptor subtypes mediating inputs to bipolar cells and ganglion cells in the tiger salamander retina. J. Neurophysiol. *69*, 2099–2107.

Ishikane, H., Gangi, M., Honda, S., and Tachibana, M. (2005). Synchronized retinal oscillations encode essential information for escape behavior in frogs. Nat. Neurosci. *8*, 1087–1095.

Jonas, P., Bischofberger, J., and Sandkuhler, J. (1998). Corelease of two fast neurotransmitters at a central synapse. Science *281*, 419–424.

Keat, J., Reinagel, P., Reid, R.C., and Meister, M. (2001). Predicting every spike: a model for the responses of visual neurons. Neuron *30*, 803–817.

Kolb, H. (1979). The inner plexiform layer in the retina of the cat: electron microscopic observations. J. Neurocytol. *8*, 295–329.

Laurent, G. (1999). A systems perspective on early olfactory coding. Science *286*, 723–728.

Magee, J.C. (2000). Dendritic integration of excitatory synaptic input. Nat. Rev. Neurosci. *1*, 181–190.

Mainen, Z.F., and Sejnowski, T.J. (1995). Reliability of spike timing in neocortical neurons. Science *268*, 1503–1506.

Matsui, K., Hosoi, N., and Tachibana, M. (1998). Excitatory synaptic transmission in the inner retina: paired recordings of bipolar cells and neurons of the ganglion cell layer. J. Neurosci. *18*, 4500–4510.

Mayer, M.L., Westbrook, G.L., and Guthrie, P.B. (1984). Voltage-dependent block by Mg2+ of NMDA responses in spinal cord neurones. Nature *309*, 261–263.

Mitchell, S.J., and Silver, R.A. (2003). Shunting inhibition modulates neuronal gain during synaptic excitation. Neuron *38*, 433–445.

Nowak, L., Bregestovski, P., Ascher, P., Herbet, A., and Prochiantz, A. (1984). Magnesium gates glutamate-activated channels in mouse central neurones. Nature *307*, 462–465.

Oertel, D. (1991). The role of intrinsic neuronal properties in the encoding of auditory information in the cochlear nuclei. Curr. Opin. Neurobiol. *1*, 221–228.

Oertel, D. (1999). The role of timing in the brain stem auditory nuclei of vertebrates. Annu. Rev. Physiol. *61*, 497–519.

Oesch, N., Euler, T., and Taylor, W.R. (2005). Direction-selective dendritic action potentials in rabbit retina. Neuron *47*, 739–750.

Olveczky, B.P., Baccus, S.A., and Meister, M. (2003). Segregation of object and background motion in the retina. Nature *423*, 401–408.

Owczarzak, M.T., and Pourcho, R.G. (1999). Transmitter-specific input to OFF-alpha ganglion cells in the cat retina. Anat. Rec. *255*, 363–373.

Pang, J.J., Gao, F., and Wu, S.M. (2003). Light-evoked excitatory and inhibitory synaptic inputs to ON and OFF alpha ganglion cells in the mouse retina. J. Neurosci. *23*, 6063–6073.

Petersen, R.S., Panzeri, S., and Diamond, M.E. (2002). Population coding in somatosensory cortex. Curr. Opin. Neurobiol. *12*, 441–447.

Pillow, J.W., Paninski, L., Uzzell, V.J., Simoncelli, E.P., and Chichilnisky, E.J. (2005). Prediction and decoding of retinal ganglion cell responses with a probabilistic spiking model. J. Neurosci. *25*, 11003–11013.

Pouille, F., and Scanziani, M. (2001). Enforcement of temporal fidelity in pyramidal cells by somatic feed-forward inhibition. Science *293*, 1159–1163.

Protti, D.A., Gerschenfeld, H.M., and Llano, I. (1997). GABAergic and glycinergic IPSCs in ganglion cells of rat retinal slices. J. Neurosci. *17*, 6075–6085.

Reich, D.S., Victor, J.D., Knight, B.W., Ozaki, T., and Kaplan, E. (1997). Response variability and timing precision of neuronal spike trains in vivo. J. Neurophysiol. *77*, 2836–2841.

Reinagel, P., and Reid, R.C. (2000). Temporal coding of visual information in the thalamus. J. Neurosci. *20*, 5392–5400.

Reyes, A. (2001). Influence of dendritic conductances on the input-output properties of neurons. Annu. Rev. Neurosci. *24*, 653–675.

Rhee, J.S., Ebihara, S., and Akaike, N. (1994). Gramicidin perforated patch-clamp technique reveals glycine-gated outward chloride current in dissociated nucleus solitarii neurons of the rat. J. Neurophysiol. *72*, 1103–1108.

Robinson, H.P., and Kawai, N. (1993). Injection of digitally synthesized synaptic conductance transients to measure the integrative properties of neurons. J. Neurosci. Methods *49*, 157–165.

Roska, B., Nemeth, E., and Werblin, F.S. (1998). Response to change is facilitated by a three-neuron disinhibitory pathway in the tiger salamander retina. J. Neurosci. *18*, 3451–3459.

Roska, B., Molnar, A., and Werblin, F.S. (2006). Parallel processing in retinal ganglion cells: how integration of space-time patterns of excitation and inhibition form the spiking output. J. Neurophysiol. *95*, 3810–3822.

Shadlen, M.N., and Newsome, W.T. (1994). Noise, neural codes and cortical organization. Curr. Opin. Neurobiol. *4*, 569–579.

Sharp, A.A., O'Neil, M.B., Abbott, L.F., and Marder, E. (1993). Dynamic clamp: computer-generated conductances in real neurons. J. Neurophysiol. *69*, 992–995.

Shu, Y., Hasenstaub, A., Badoual, M., Bal, T., and McCormick, D.A. (2003). Barrages of synaptic activity control the gain and sensitivity of cortical neurons. J. Neurosci. *23*, 10388–10401.

Softky, W.R., and Koch, C. (1993). The highly irregular firing of cortical cells is inconsistent with temporal integration of random EPSPs. J. Neurosci. *13*, 334–350.

Strettoi, E., Raviola, E., and Dacheux, R.F. (1992). Synaptic connections of the narrow-field, bistratified rod amacrine cell (AII) in the rabbit retina. J. Comp. Neurol. *325*, 152–168.

Stuart, G., Spruston, N., and Hausser, M. (2000). Dendrites (New York: Oxford University Press).

Trussell, L.O. (1997). Cellular mechanisms for preservation of timing in central auditory pathways. Curr. Opin. Neurobiol. *7*, 487–492.

Uzzell, V.J., and Chichilnisky, E.J. (2004). Precision of spike trains in primate retinal ganglion cells. J. Neurophysiol. *92*, 780–789.

Victor, J.D., and Purpura, K.P. (1996). Nature and precision of temporal coding in visual cortex: a metric-space analysis. J. Neurophysiol. *76*, 1310–1326.

Volgyi, B., Deans, M.R., Paul, D.L., and Bloomfield, S.A. (2004). Convergence and segregation of the multiple rod pathways in mammalian retina. J. Neurosci. *24*, 11182–11192.

Wassle, H., Koulen, P., Brandstatter, J.H., Fletcher, E.L., and Becker, C.M. (1998). Glycine and GABA receptors in the mammalian retina. Vision Res. *38*, 1411–1430.

Wehr, M., and Zador, A.M. (2003). Balanced inhibition underlies tuning and sharpens spike timing in auditory cortex. Nature *426*, 442–446.

White, J.A., Rubinstein, J.T., and Kay, A.R. (2000). Channel noise in neurons. Trends Neurosci. *23*, 131–137.

Zaghloul, K.A., Boahen, K., and Demb, J.B. (2003). Different circuits for ON and OFF retinal ganglion cells cause different contrast sensitivities. J. Neurosci. *23*, 2645–2654.

Zsiros, V., and Hestrin, S. (2005). Background synaptic conductance and precision of EPSP-spike coupling at pyramidal cells. J. Neurophysiol. *93*, 3248–3256.